How to cite: *Angew. Chem. Int. Ed.* **2023,** *62,* e202218539
International Edition: doi.org/10.1002/anie.202218539
German Edition: doi.org/10.1002/ange.202218539

Gas-Phase Chemistry

CO_2 Aggregation on Monoethanolamine: Observations from Rotational Spectroscopy

*Fan Xie, Wenhao Sun, Pablo Pinacho, and Melanie Schnell**

Abstract: The initial stages of the gas-phase nucleation between CO_2 and monoethanolamine were investigated via broadband rotational spectroscopy with the aid of extensive theoretical structure sampling. Sub-nanometer-scale aggregation patterns of monoethanolamine-$(CO_2)_n$, $n=1$–4, were identified. An interesting competition between the monoethanolamine intramolecular hydrogen bond and the intermolecular interactions between monoethanolamine and CO_2 upon cluster growth was discovered, revealing an intriguing CO_2 binding priority to the hydroxyl group over the amine group. These findings are in sharp contrast to the general results for aqueous solutions. In the quinary complex, a cap-like CO_2 tetramer was observed cooperatively surrounding the monoethanolamine. As the cluster approaches the critical size of new particle formation, the contribution of CO_2 self-assembly to the overall stability increases.

Introduction

Human-induced climate change has attracted wide attention for its foreseeable catastrophic consequences.[1] Ever frequent extreme weather events such as heat waves were linked with the rising global average temperature.[2] Among the greenhouse gases, CO_2 contributes more than 60% to global warming.[3] To date, the peak CO_2 concentration in the atmosphere has reached 421 ppm, which is 50% higher than pre-industrial levels according to the Mauna Loa Observatory.[4] In response to the growing climate change induced by human activities, nations and organizations across the world have declared to achieve carbon neutrality within the next few decades.[5]

[*] Dr. F. Xie, Dr. W. Sun, Dr. P. Pinacho, Prof. Dr. M. Schnell
Deutsches Elektronen-Synchrotron DESY
Notkestr. 85, 22607 Hamburg (Germany)
E-mail: melanie.schnell@desy.de
Prof. Dr. M. Schnell
Institut für Physikalische Chemie,
Christian-Albrechts-Universität zu Kiel
Max-Eyth-Str. 1, 24118 Kiel (Germany)

One of the essential measures is to develop technologies to capture and store CO_2.[6] Aqueous alkanolamine solutions are already commercialized in removing trace CO_2 from flue gas and natural gas.[7] It is also expected to be the most applicable molecular system for absorbing the CO_2 emission of power plants.[6,8] Among the various alkanolamines, monoethanolamine (MEA), in particular, serves as a benchmark system, and its reaction mechanism and kinetic behaviors were extensively studied by quantum-chemical calculations and nuclear magnetic resonance spectroscopy.[9] It is commonly assumed that a key intermediate of the reaction is a zwitterion formed via the attack from the NH_2 lone pair to the electron deficient CO_2 carbon atom. Despite enormous theoretical investigations that were performed,[9b,c,10] the zwitterion has not been experimentally observed to date. Furthermore, physical/chemical adsorption of CO_2 on porous nanomaterials has attracted significant interest for its inherent low energy consumption in regeneration and gentle corrosivity compared to the alkanolamine solutions. Various adsorbents, for example functionalized graphene,[11] carbon nanotubes (CNT),[12] or amine-containing metal–organic frameworks (MOFs),[11,13] were proposed and tested.

With respect to atmospheric chemistry, CO_2 was used as a prototype molecular system to study nucleation processes in the gas phase.[14] The kinetic behaviors and shell structures of nanometer scale clusters were extensively characterized via laser-coupled mass spectrometry.[15] It was discovered that the presence of weakly bonded CO_2 hetero-molecular clusters was able to efficiently catalyze aerosol formation,[16] despite the exact intermolecular binding topology remaining unknown due to the complexity of the nearly condensed particles and the lack of structure sensitivity of the applied detection methods.[17]

High-resolution molecular spectroscopy is well known for its ability to provide accurate, structure-specific characterization of smaller weakly bound complexes that could be present in the initial stages of aerosol formation.[18] For example, self-aggregation processes of neutral CO_2 with up to thirteen partners were revealed using jet-expansion infrared spectroscopy.[19] The complexes between CO_2 and other linear molecules such as HCN, OCS, N_2O, and CS_2 were also studied via infrared and microwave spectroscopy.[19a] With water participating, microhydration topologies of CO_2 and MEA were revealed by the observation of noncovalently bonded complexes.[20] Recently, insights into noncovalent interactions between CO_2 and complex partner molecules containing various func-

tional groups including NH_2, OH, C=O, ether, and aryl were systematically gained via rotational spectroscopy.[21]

In this study, we present the direct observation of sub-nanometer scale CO_2 aggregation processes on MEA using broadband chirped-pulse Fourier transform microwave (CP-FTMW) spectroscopy, also known as Molecular Rotational Resonance spectroscopy[22] combined with high-level theoretical calculations. An interesting competition between the MEA intramolecular hydrogen bond (H-bond) and the intermolecular interactions between MEA and CO_2 upon cluster growth was discovered revealing the aggregation pattern of early-stage gas-phase nucleation.

Results and Discussion

The measurements were carried out using the Hamburg CP-FTMW spectrometer COMPACT (compact-passage-acquired coherence-technique) covering the 2–8 GHz frequency range.[23] The detailed operating principle and device specifications are described elsewhere.[23] Here a brief description of the experimental details is provided. An approximate concentration of 1 % of CO_2 was seeded in neon as carrier gas at a backing pressure of 3 bars. MEA (98 % chemical purity) was purchased from Sigma–Aldrich and used without further purifications. The liquid MEA sample was placed in a homemade internal reservoir located directly at the valve orifice before the jet expansion and heated up to 50 °C. A supersonic jet was generated by the adiabatic expansion of the gas mixture of diluted MEA and CO_2 into a vacuum chamber. Since trace water vapor is ubiquitous in the pipe lines of the instrument, the spectra of pure MEA and CO_2 were measured separately with slightly hydrated neon carrier gas. These spectra were used as background spectra to isolate the rotational fingerprints of the targeted MEA-$(CO_2)_n$ clusters from the complicated global spectrum that is dominated by MEA monomers, possible MEA hydrates as well as CO_2 hydrates in different combination degrees. For each measurement, about four million acquisitions in the form of a free induction decay (FID) (see experimental details in the Supporting Information) were collected and averaged.

To aid the identification of the MEA-$(CO_2)_n$ cluster binding topologies, an increasingly popular scheme[24] combining the cost-effective conformational space exploration tool CREST[25] with quantum-chemical calculations was applied. Low-energy isomers obtained using the GFN2-xTB[26] approach were used as starting geometries of B3LYP-D3(BJ)/def2-TZVP[27] re-optimizations using the ORCA quantum-chemistry program package.[28] Harmonic frequency calculations were carried out to verify these geometries to be real minima and to provide zero-point-energy (ZPE) corrections. The list of the energetically low-lying conformational ensemble of MEA-$(CO_2)_n$, $n=1$–4, and their corresponding spectroscopic constants are listed in Table S1 in the Supporting Information.

After subtraction of the background spectra, as discussed above, a set of strong a-type transitions was assigned in the experimental spectrum (Figure 1 (a)), which could be identified as the MEA-CO_2 dimer based on the magnitude of the fitted rotational constants. However, we were unable to find a satisfactory match with any of the calculated spectroscopic constants of the isomers, obtained at the B3LYP-D3(BJ)/def2-TZVP level of theory as presented in the Supporting Information, Table S1, despite exhaustive structural searches. This situation led us to search for the spectral signatures of the singly substituted heavy-atom isotopologues in natural abundance (i.e., ^{15}N and ^{13}C), thereby determining the structure of the heavy-atom backbone experimentally. The spectra of ^{13}C and ^{15}N singly substituted MEA-CO_2 in natural abundance were readily visible and assigned after 16 million FIDs were accumulated in an additional measurement. The fitted spectroscopic constants, derived Kraitchman coordinates,[29] and rotational transitions included in the fits are summarized in the Supporting Information, Tables S2, S3, and S7, respectively.

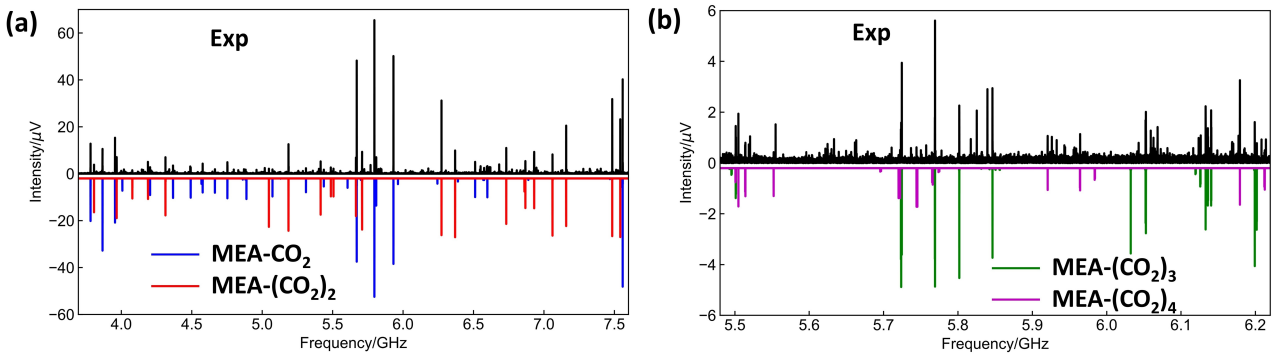

Figure 1. Sections of the broadband rotational spectrum for MEA-CO_2 clusters. (a) Broad overview of the experimental spectrum (black trace) and simulated spectra of MEA-CO_2 (blue trace) and MEA-$(CO_2)_2$ (red trace) based on the fitted experimental rotational constants. (b) Zoom-in section of the experimental spectrum (black trace) to highlight larger MEA-CO_2 clusters together with the simulated spectra for MEA-$(CO_2)_3$ (green trace) and MEA-$(CO_2)_4$ (purple trace) based on the fitted experimental rotational constants. For all the simulations, a rotational temperature of 1 K was used.

An interesting binding topology between CO_2 and MEA emerged based on the determined experimental structure, as illustrated in Figure 2. Two oxygen lone pairs of the OH group of MEA competitively bind to the electron-deficient carbon atom of CO_2. This observation inspired us to perform a relaxed scan at multiple levels of theory as a function of the C–C–C angle, in which the CO_2 binding site shifts from one OH lone pair to the other. Both the B3LYP-D3(BJ)/def2-TZVP and MP2/def2-TZVP[30] energy scans predicted a stability priority of a single lone-pair binding topology that adopts a C–C–C angle of 96°, while the other single lone pair binding configuration of 150° is about 1 kJ mol^{-1} higher in energy. Note that these two lone-pair binding sites are calculated to be almost isoenergetic at the DLPNO-CCSD(T)[31]/CBS(3/4)[32] level, and the minimum structure adopts an intermediate angle of 120° that is close to the angle of 122.91(56)° derived from the Kraitchman structure[29] via rotational spectroscopy. Based on this, we decided to perform a more expensive geometry optimization of the MEA-CO_2 dimer at the DLPNO-CCSD(T)/cc-pVQZ level of theory. The calculated spectroscopic constants agree with the experimental values reasonably well, as shown in Table 1.

After the rotational transitions corresponding to the MEA-CO_2 dimer have been identified in the spectrum, another set of slightly weaker a-type transitions could be assigned, this set could be identified as MEA-$(CO_2)_2$ (red trace in Figure 1 (a)) by comparison with the results from quantum-chemical calculations (Table S1) as well as the overall magnitude of the rotational constants. After removing the transitions for both MEA-CO_2 and MEA-$(CO_2)_2$, another two sets of weak b-type transitions were identified as MEA-$(CO_2)_3$ and MEA-$(CO_2)_4$, respectively, with an overview of the spectrum presented in Figure 1 (b). From the isomeric ensembles of MEA-$(CO_2)_n$, $n=2$–4, optimized at the B3LYP-D3(BJ)/def2-TZVP level and presented in the Supporting Information, Table S1, we were able to identify cluster structures that unambiguously match with the experimentally determined spectroscopic constants including the rotational constants, the ^{14}N nuclear quadrupole coupling constants, and the magnitudes of the electric dipole-moment components as compared in Table 1. The complete set of fitted constants and rotational transitions included in the fits are presented in the Supporting Information, Tables S4 and S6, respectively. According to the single-point energies obtained using DLPNO-CCSD(T)/CBS(3/4), the observed structures of MEA-$(CO_2)_n$, $n=$ 2–4, are the global minima of their respective isomer pool, which is consistent with the characteristics of supersonic jet expansion experiments.

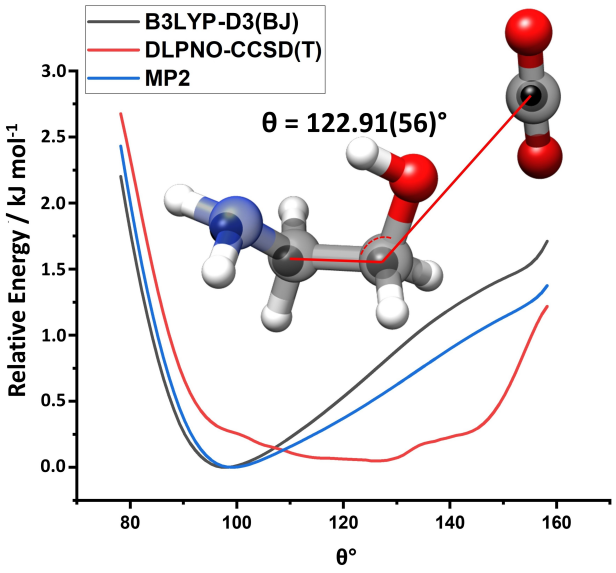

Figure 2. The relaxed energy scan profile as a function of the angle of the three carbon atoms, ranging from 80° to 160° at the B3LYP-D3(BJ)/def2-TZVP (black) and MP2/def2-TZVP (blue) levels of theory with a step size of 1°. The energy curve in red was assembled using single-point energies obtained with DLPNO-CCSD(T)/CBS(3/4) on the structures of 80 constrained optimizations from the relaxed B3LYP-D3(BJ)/def2-TZVP scan. In the molecular structure of MEA-CO_2, the Kraitchman coordinates obtained from the analysis of the ^{13}C and ^{15}N singly substituted isotopologues were indicated with solid black balls. The corresponding angle determined via rotational spectroscopy is 122.91(56)°.

The experimentally identified structures of MEA-$(CO_2)_n$, $n=1$–4, together with their visualized non-covalent interactions (NCI)[35] using Multiwfn,[36] are summarized in Figure 3. The predominant contributions of CO_2 binding to MEA arise from the OH or NH_2 lone pairs binding with the electron-deficient center of CO_2. This meets the definition of a O–C or N–C tetrel bond.[37] They are indicated with light blue isosurfaces. Additionally, weaker van der Waals interactions marked with green color could be found between the MEA hydrogen atoms and the CO_2 lone pairs. In the structure of MEA-CO_2, both lone pairs of the OH group competitively bind to the CO_2 molecule, revealing the inadequacy of relative energy calculations at both the B3LYP-D3(BJ) and MP2 levels as discussed above. With one more CO_2 participating in the complexation of MEA-$(CO_2)_2$, each of the OH lone pairs is occupied by one of the electron-deficient centers of the distorted CO_2 dimer. In such cases, geometries optimized at the B3LYP-D3(BJ)/def2-TZVP level of theory were sufficient enough to provide unambiguous agreement with the experimentally determined spectroscopic constants and thus confident structural assignments. With both OH lone pairs occupied, the third CO_2 molecule attaches to the NH_2 group, interacting with the moderate intramolecular H-bond between the NH_2 and the OH group. In the structure of MEA-$(CO_2)_3$, the bifurcation of the NH_2 lone pair is evident, both the electron-deficient CO_2 carbon atom and the OH proton competitively serve as the electron-density acceptors. Interestingly, such bifurcated binding topologies can also be found in the calculated isomeric ensemble of MEA-$(CO_2)_n$, $n=1,2,4$. They are the second most stable structures within their respective isomer pool according to DLPNO-CCSD(T)/CBS(3/4) energies. A comparison of these complexation patterns, relative stabilities, and SAPT[38] energy decomposition of the intramolecular H-

Table 1: Comparison between experimentally determined and calculated rotational parameters of MEA-$(CO_2)_n$, $n=1$–4. *A*, *B*, and *C* are the rotational constants, μ_a, μ_b and μ_c are the electric dipole-moment components. *N* is the number of rotational transitions included in the fit. σ is the root-mean-square deviation of the fit. Watson's semirigid-rotor *S*-reduction Hamiltonian[33] coupled with one nitrogen hyperfine term in its *I*′ representation was applied to the assignments using PGOPHER.[34]

	MEA-CO_2	Calc.[a]	MEA-$(CO_2)_2$	Calc.[b]	MEA-$(CO_2)_3$	Calc.[b]	MEA-$(CO_2)_4$	Calc.[b]
A/MHz	5587.6366(15)	5396	1417.6677(10)	1418	887.70093(44)	917	487.48066(37)	498
B/MHz	1010.4417(5)	1038	764.75327(63)	772	471.11789(30)	465	414.68096(98)	416
C/MHz	923.5907(5)	943	594.66506(49)	603	399.81649(24)	404	337.30392(22)	341
χ_{aa}/MHz	−0.8296(44)	−1.27	−1.7623(43)	−2.5	2.0996(75)	2.6	2.083(29)	1.4
χ_{bb}–χ_{cc}/MHz	−1.8537(72)	−2.53	1.8011(92)	2.1	−2.049(11)	−3.6	−4.338(33)	−4.5
|Dipole moment|/Debye	$\mu_a > \mu_b \approx \mu_c$	3.6/0.7/0.7	μ_a, no μ_b, μ_c	3.8/0.4/0.4	$\mu_a \approx \mu_b$, no μ_c	2.1/2.6/0.7	μ_b, no μ_a μ_c	2.0/3.2/0.1
N	94	–	88	–	171	–	111	–
σ/kHz	6.8	–	6.1	–	6.7	–	6.3	–

[a] Calculated spectroscopic constants of the minimum structure optimized at the DLPNO-CCSD(T)/cc-pVQZ level of theory. [b] The rotational constants were calculated from minimum structures optimized at the B3LYP-D3(BJ)/def2-TZVP level of theory. The dipole-moment components and nitrogen hyperfine constants were derived from the electronic configurations of DLPNO-CCSD(T)/CBS(3/4) single-point energy calculations using the geometries optimized at the B3LYP-D3(BJ)/def2-TZVP level.

bond strength is provided in Figure S3 and Table S5. It should be noted that the stability priority of fully O–C tetrel bonded structure is pronounced only in MEA-CO_2 and MEA-$(CO_2)_2$. With the third and fourth CO_2 aggregate on MEA, hybrid O–C and N–C binding topologies begin to show competitiveness.

As the aggregation is progressing, the self-binding interactions between CO_2 molecules become readily visible according to the NCI representations. The observed MEA-$(CO_2)_4$ complex configuration is a particularly interesting case: a three-dimensional van der Waals interaction network is constructed by the interactions between the electron lone pairs of the CO_2 oxygen atoms and the electron-deficient carbon atoms of neighboring CO_2 molecules. Each of the CO_2 bridges with two or three other CO_2 molecules, whereas such self-aggregation was observed in a one-on-one fashion for the configurations of MEA-$(CO_2)_2$ and MEA-$(CO_2)_3$. In order to quantitively analyze the interaction strength with increasing level of aggregation and the partition of the CO_2 self-binding energies contributing to the global stability, a simple energy decomposition scheme is applied for observed MEA-$(CO_2)_n$, $n=1$–4, with the detailed formalism explained in the Supporting Information. The averaged total interaction energies (black) and interaction energies between MEA and CO_2 (red) calculated at DLPNO-CCSD(T)/CBS(3/4) level of theory are summarized in Figure 4. The energy gap (green) between them represents the CO_2 self-binding energies. With more CO_2 molecules aggregating on MEA, an increasing trend of CO_2 self-interaction strength is evident. Especially in the case of MEA-$(CO_2)_4$, 28 % of interaction energy is contributed from CO_2 self-assembling.

Conclusion

The spectroscopic identification of the $(CO_2)_n$, $n=1$–4, aggregation pattern on MEA was performed with the aid of extensive theoretical calculations. The relatively expensive DLPNO-CCSD(T) level of theory is necessary to rationalize the observations in the delicate case of the mono-CO_2 aggregation, resulting in the MEA-CO_2 dimer. Without the participation of water,[20d] we found that the binding topology between CO_2 and NH_2 that leads to the formation of the zwitterionic intermediate in aqueous solutions is not populated under molecular-jet expansion conditions, since the NH_2 was predominantly occupied by the intramolecular H-bond. Instead, O–C tetrel bonding was observed with energetic preference, especially in the first and second CO_2 aggregation. These observed aggregation patterns from binary to quinary complexes in the gas phase could support the understanding of the building-up processes of aerosols that are formed in the amine scrubbing process.[39] Furthermore, the variation of the interaction strength and the role of CO_2 self-aggregation along the aggregation process were revealed, providing insights into the future design of high-capacity CO_2 capture materials.

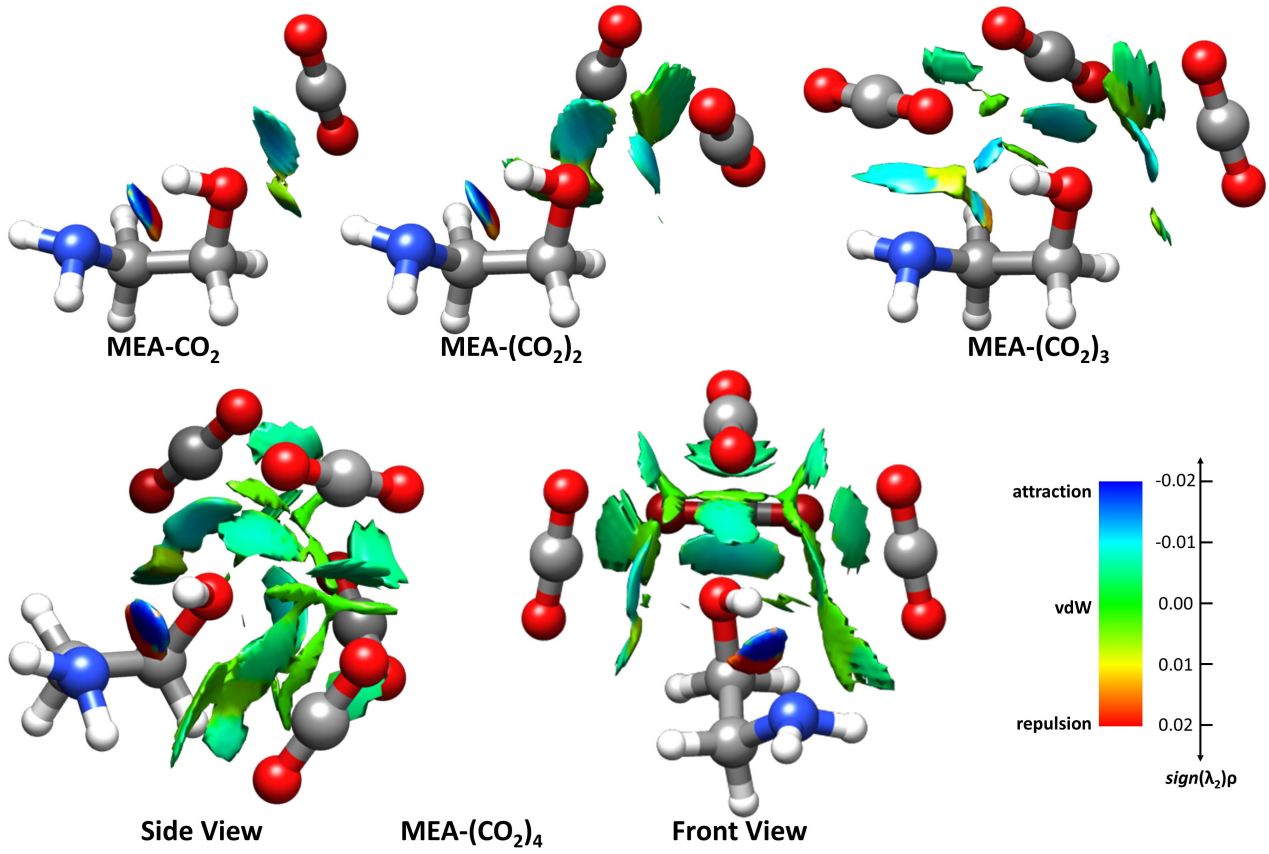

Figure 3. Binding topologies and NCI plots of the observed MEA-$(CO_2)_n$, $n=1$–4, complexes. The structure of MEA-CO_2 is optimized at the DLPNO-CCSD(T)/cc-pVQZ level. The structures of MEA-$(CO_2)_n$, $n=2$–4, are optimized at B3LYP-D3(BJ)/def2-TZVP level. The isosurface cut-off value is 0.6. The attractive and repulsive interactions are defined by the sign of sign$(\lambda_2)\varrho$, λ_2 is the second eigenvalue of the electron-density Hessian. ϱ is the electron density. As indicated in the color bar, deep blue represents strong attractive interactions, light blue indicates a moderate attractive interaction, and weaker van der Waals (vdW) interactions are colored in green.

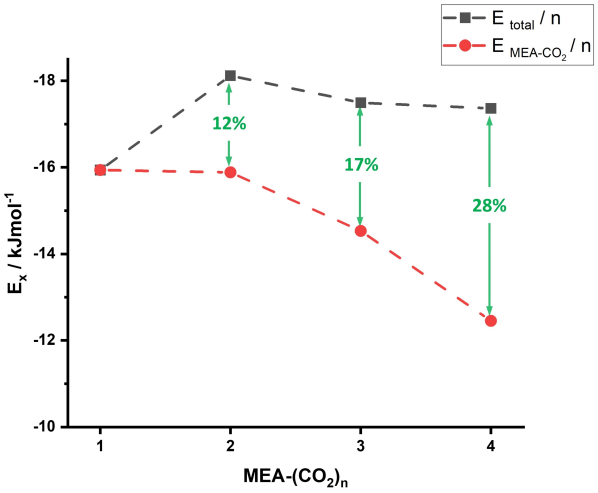

Figure 4. The decomposition of total interaction energy E_{total} (black) into MEA-CO_2 interaction energy (red) and CO_2 self-binding energy (green) calculated using the DLPNO-CCSD(T)/CBS(3/4) single-point energies.

Acknowledgements

F. X. acknowledges the support of Alexander von Humboldt postdoctoral fellowships. We acknowledge the detailed guidance of high-level quantum-chemical calculations from Dr. Denis Tikhonov. Open Access funding enabled and organized by Projekt DEAL.

Conflict of Interest

The authors declare no conflict of interest.

Data Availability Statement

The data that support the findings of this study are available in the supplementary material of this article.

Keywords: Aerosol Formation · CO_2 Complexes · Molecular Interactions · Rotational Spectroscopy

[1] P. Stott, *Science* **2016**, *352*, 1517–1518.
[2] a) O. Deschênes, E. Moretti, *Rev. Econ. Stat.* **2009**, *91*, 659–681; b) J. M. Wallace, I. M. Held, D. W. Thompson, K. E. Trenberth, J. E. Walsh, *Science* **2014**, *343*, 729–730.
[3] H. Ritchie, M. Roser, P. Rosado, *Our world in data* **2020**, https://ourworldindata.org/energy.
[4] R. E. Stumm, *ASHRAE J.* **2022**, *64*, 14–22.
[5] a) Z. Liu, Z. Deng, G. He, H. Wang, X. Zhang, J. Lin, Y. Qi, X. Liang, *Nat. Rev. Earth Environ.* **2022**, *3*, 141–155; b) L. De La Peña, R. Guo, X. Cao, X. Ni, W. Zhang, *Resour. Conserv. Recycl.* **2022**, *177*, 105957.
[6] C. H. Yu, C. H. Huang, C. S. Tan, *Aerosol Air Qual. Res.* **2012**, *12*, 745–769.
[7] P. Feron in *Absorption-based post-combustion capture of carbon dioxide*, Woodhead publishing, London, **2016**. pp. 35–65.
[8] G. T. Rochelle, *Science* **2009**, *325*, 1652–1654.
[9] a) G. S. Hwang, H. M. Stowe, E. Paek, D. Manogaran, *Phys. Chem. Chem. Phys.* **2015**, *17*, 831–839; b) Y. Kubota, T. Ohnuma, T. Bučko, *J. Chem. Phys.* **2017**, *146*, 094303; c) H. Xie, P. Wang, N. He, X. Yang, J. Chen, *J. Environ. Sci.* **2015**, *37*, 75–82; d) H.-B. Xie, Y. Zhou, Y. Zhang, J. K. Johnson, *J. Phys. Chem. A* **2010**, *114*, 11844–11852; e) B. Lv, B. Guo, Z. Zhou, G. Jing, *Environ. Sci. Technol.* **2015**, *49*, 10728–10735.
[10] Y. Kubota, T. Bučko, *J. Chem. Phys.* **2018**, *149*, 224103.
[11] D. Saha, Z. Bao, F. Jia, S. Deng, *Environ. Sci. Technol.* **2010**, *44*, 1820–1826.
[12] a) M. Cinke, J. Li, C. W. Bauschlicher Jr, A. Ricca, M. Meyyappan, *Chem. Phys. Lett.* **2003**, *376*, 761–766; b) J. Li, Y. Lu, Q. Ye, M. Cinke, J. Han, M. Meyyappan, *Nano Lett.* **2003**, *3*, 929–933.
[13] a) E. A. Quadrelli, G. Centi, J. L. Duplan, S. Perathoner, *ChemSusChem* **2011**, *4*, 1194–1215; b) E. S. Sanz-Pérez, C. R. Murdock, S. A. Didas, C. W. Jones, *Chem. Rev.* **2016**, *116*, 11840–11876; c) T. M. McDonald, J. A. Mason, X. Kong, E. D. Bloch, D. Gygi, A. Dani, V. Crocella, F. Giordanino, S. O. Odoh, W. S. Drisdell, *Nature* **2015**, *519*, 303–308; d) Y. Fu, D. Sun, Y. Chen, R. Huang, Z. Ding, X. Fu, Z. Li, *Angew. Chem. Int. Ed.* **2012**, *51*, 3364–3367; *Angew. Chem.* **2012**, *124*, 3420–3423; e) R. W. Flaig, T. M. Osborn Popp, A. M. Fracaroli, E. A. Kapustin, M. J. Kalmutzki, R. M. Altamimi, F. Fathieh, J. A. Reimer, O. M. Yaghi, *J. Am. Chem. Soc.* **2017**, *139*, 12125–12128; f) Y. Lin, C. Kong, L. Chen, *RSC Adv.* **2016**, *6*, 32598–32614; g) R. Vaidhyanathan, S. S. Iremonger, K. W. Dawson, G. K. Shimizu, *Chem. Commun.* **2009**, 5230–5232; h) B. Arstad, H. Fjellvåg, K. O. Kongshaug, O. Swang, R. Blom, *Adsorption* **2008**, *14*, 755–762.
[14] C. Li, R. Signorell, *J. Aerosol Sci.* **2021**, *153*, 105676.
[15] J. W. Niman, B. S. Kamerin, V. V. Kresin, J. Krohn, R. Signorell, R. Halonen, K. Hansen, *Phys. Chem. Chem. Phys.* **2022**, *24*, 5343–5350.
[16] C. Li, J. Krohn, M. Lippe, R. Signorell, *Sci. Adv.* **2021**, *7*, eabd9954.
[17] a) M. Kulmala, I. Riipinen, M. Sipilä, H. E. Manninen, T. Petäjä, H. Junninen, M. D. Maso, G. Mordas, A. Mirme, M. Vana, *Science* **2007**, *318*, 89–92; b) M. Kulmala, J. Kontkanen, H. Junninen, K. Lehtipalo, H. E. Manninen, T. Nieminen, T. Petäjä, M. Sipilä, S. Schobesberger, P. Rantala, *Science* **2013**, *339*, 943–946.
[18] a) C. Wang, L. Fu, S. Yang, H. Zheng, T. Wang, J. Gao, M. Su, J. Yang, G. Wu, W. Zhang, *J. Phys. Chem. Lett.* **2022**, *13*, 5654–5659; b) R. B. Mackenzie, C. T. Dewberry, K. R. Leopold, *Science* **2015**, *349*, 58–61.
[19] a) N. Moazzen-Ahmadi, A. McKellar, *Int. Rev. Phys. Chem.* **2013**, *32*, 611–650; b) J. N. Oliaee, M. Dehghany, N. Moazzen-Ahmadi, A. McKellar, *Phys. Chem. Chem. Phys.* **2011**, *13*, 1297–1300; c) J. Norooz Oliaee, M. Dehghany, A. McKellar, N. Moazzen-Ahmadi, *J. Chem. Phys.* **2011**, *135*, 044315; d) M. J. Weida, D. J. Nesbitt, *J. Chem. Phys.* **1996**, *105*, 10210–10223; e) M. Dehghany, M. Afshari, N. Moazzen-Ahmadi, A. McKellar, *J. Chem. Phys.* **2008**, *128*, 064308; f) M. J. Weida, J. M. Sperhac, D. J. Nesbitt, *J. Chem. Phys.* **1995**, *103*, 7685–7699; g) G. Fraser, A. Pine, W. Lafferty, R. Miller, *J. Chem. Phys.* **1987**, *87*, 1502–1508; h) M. Walsh, T. England, T. Dyke, B. Howard, *Chem. Phys. Lett.* **1987**, *142*, 265–270; i) K. Jucks, Z. Huang, R. Miller, G. Fraser, A. Pine, W. Lafferty, *J. Chem. Phys.* **1988**, *88*, 2185–2195.
[20] a) K. Peterson, R. Suenram, F. Lovas, *J. Chem. Phys.* **1989**, *90*, 5964–5970; b) K. Peterson, R. Suenram, F. J. Lovas, *J. Chem. Phys.* **1991**, *94*, 106–117; c) A. Davis, B. Oliver, *J. Solution Chem.* **1972**, *1*, 329–339; d) M. J. Tubergen, C. R. Torok, R. J. Lavrich, *J. Chem. Phys.* **2003**, *119*, 8397–8403.
[21] a) H. Wang, J. Chen, W. Cheng, Y. Zheng, S. Zou, W. Du, X. Xu, Q. Gou, *Spectrochim. Acta Part A* **2022**, *282*, 121677; b) H. Wang, J. Chen, Y. Zheng, D. A. Obenchain, X. Xu, Q. Gou, J.-U. Grabow, W. Caminati, *J. Phys. Chem. Lett.* **2022**, *13*, 149–155; c) H. Wang, X. Wang, X. Tian, W. Cheng, Y. Zheng, D. A. Obenchain, X. Xu, Q. Gou, *Phys. Chem. Chem. Phys.* **2021**, *23*, 25784–25788; d) S. Gao, D. A. Obenchain, J. Lei, G. Feng, S. Herbers, Q. Gou, J.-U. Grabow, *Phys. Chem. Chem. Phys.* **2019**, *21*, 7016–7020; e) M. Li, J. Lei, G. Feng, J.-U. Grabow, Q. Gou, *Spectrochim. Acta Part A* **2020**, *238*, 118424; f) T. Lu, J. Zhang, Q. Gou, G. Feng, *Phys. Chem. Chem. Phys.* **2020**, *22*, 8467–8475; g) R. A. Peebles, S. A. Peebles, A. M. Anderton, C. L. Christenholz, R. E. Dorris, W. C. Trendell, in *254th American Chemical Society National Meeting*, **2017**; h) P. B. Kannangara, C. T. West, S. A. Peebles, R. A. Peebles, *Chem. Phys. Lett.* **2018**, *706*, 538–542.
[22] a) G. G. Brown, B. C. Dian, K. O. Douglass, S. M. Geyer, S. T. Shipman, B. H. Pate, *Rev. Sci. Instrum.* **2008**, *79*, 053103; b) G. G. Brown, B. C. Dian, K. O. Douglass, S. M. Geyer, B. H. Pate, *J. Mol. Spectrosc.* **2006**, *238*, 200–212; c) G. B. Park, R. W. Field, *J. Chem. Phys.* **2016**, *144*, 200901.
[23] D. Schmitz, V. A. Shubert, T. Betz, M. Schnell, *J. Mol. Spectrosc.* **2012**, *280*, 77–84.
[24] a) F. Xie, X. Ng, N. A. Seifert, J. Thomas, W. Jäger, Y. Xu, *J. Chem. Phys.* **2018**, *149*, 224306; b) F. Xie, N. A. Seifert, M. Heger, J. Thomas, W. Jäger, Y. Xu, *Phys. Chem. Chem. Phys.* **2019**, *21*, 15408–15416; c) F. Xie, N. A. Seifert, W. Jäger, Y. Xu, *Angew. Chem. Int. Ed.* **2020**, *59*, 15703–15710; *Angew. Chem.* **2020**, *132*, 15833–15840; d) F. Xie, M. Fusè, A. S. Hazrah, W. Jäger, V. Barone, Y. Xu, *Angew. Chem. Int. Ed.* **2020**, *59*, 22427; *Angew. Chem.* **2020**, *132*, 22613; e) E. Burevschi, I. Peña, M. E. Sanz, *J. Phys. Chem. Lett.* **2021**, *12*, 12419–12425; f) W. G. Silva, T. Poonia, J. van Wijngaarden, *ChemPhysChem* **2020**, *21*, 2515–2522; g) W. Li, M. M. Quesada-Moreno, P. Pinacho, M. Schnell, *Angew. Chem. Int. Ed.* **2021**, *60*, 5323; *Angew. Chem.* **2021**, *133*, 5383.
[25] a) S. Grimme, C. Bannwarth, P. Shushkov, *J. Chem. Theory Comput.* **2017**, *13*, 1989–2009; b) P. Pracht, F. Bohle, S. Grimme, *Phys. Chem. Chem. Phys.* **2020**, *22*, 7169–7192; c) S. Grimme, *J. Chem. Theory Comput.* **2019**, *15*, 2847–2862.
[26] C. Bannwarth, S. Ehlert, S. Grimme, *J. Chem. Theory Comput.* **2019**, *15*, 1652–1671.
[27] a) S. Grimme, S. Ehrlich, L. Goerigk, *J. Comput. Chem.* **2011**, *32*, 1456–1465; b) E. Caldeweyher, S. Ehlert, A. Hansen, H. Neugebauer, S. Spicher, C. Bannwarth, S. Grimme, *J. Chem. Phys.* **2019**, *150*, 154122; c) D. G. Smith, L. A. Burns, K. Patkowski, C. D. Sherrill, *J. Phys. Chem. Lett.* **2016**, *7*, 2197–2203; d) C. Lee, W. Yang, R. G. Parr, *Phys. Rev. B* **1988**, *37*, 785; e) A. D. Becke, *J. Chem. Phys.* **1992**, *96*, 2155–2160; f) F. Weigend, R. Ahlrichs, *Phys. Chem. Chem. Phys.* **2005**, *7*, 3297–3305; g) F. Weigend, *Phys. Chem. Chem. Phys.* **2006**, *8*, 1057–

1065; h) R. A. Kendall, T. H. Dunning Jr, R. J. Harrison, *J. Chem. Phys.* **1992**, *96*, 6796–6806; i) T. H. Dunning Jr, *J. Chem. Phys.* **1989**, *90*, 1007–1023.
[28] a) F. Neese, *Wiley Interdiscip. Rev.: Comput. Mol. Sci.* **2012**, *2*, 73–78; b) F. Neese, *Wiley Interdiscip. Rev.: Comput. Mol. Sci.* **2022**, *12*, e1606; c) F. Neese, F. Wennmohs, U. Becker, C. Riplinger, *J. Chem. Phys.* **2020**, *152*, 224108.
[29] J. Kraitchman, *Am. J. Phys.* **1953**, *21*, 17–24.
[30] a) M. Head-Gordon, J. A. Pople, M. J. Frisch, *Chem. Phys. Lett.* **1988**, *153*, 503–506; b) M. Feyereisen, G. Fitzgerald, A. Komornicki, *Chem. Phys. Lett.* **1993**, *208*, 359–363.
[31] a) D. G. Liakos, F. Neese, *J. Chem. Theory Comput.* **2015**, *11*, 4054–4063; b) O. Demel, J. Pittner, F. Neese, *J. Chem. Theory Comput.* **2015**, *11*, 3104–3114.
[32] F. Neese, A. Hansen, D. G. Liakos, *J. Chem. Phys.* **2009**, *131*, 064103.
[33] J. K. Watson, in *Vibrational spectra and structure*, Elsevier, Amsterdam, **1977**.
[34] C. M. Western, *J. Quant. Spectrosc. Radiat. Transfer* **2017**, *186*, 221–242.
[35] E. R. Johnson, S. Keinan, P. Mori-Sánchez, J. Contreras-García, A. J. Cohen, W. Yang, *J. Am. Chem. Soc.* **2010**, *132*, 6498–6506.
[36] T. Lu, F. Chen, *J. Comput. Chem.* **2012**, *33*, 580–592.
[37] a) A. Bauzá, T. J. Mooibroek, A. Frontera, *Angew. Chem. Int. Ed.* **2013**, *52*, 12317–12321; *Angew. Chem.* **2013**, *125*, 12543–12547; b) D. Mani, E. Arunan, *Phys. Chem. Chem. Phys.* **2013**, *15*, 14377–14383; c) S. P. Gnanasekar, E. Arunan, *J. Mol. Spectrosc.* **2022**, *388*, 111671.
[38] a) S. Scheiner, in *Hydrogen Bonding: A Theoretical Perspective*, Oxford University Press, Oxford, **1997**; b) B. Jeziorski, R. Moszynski, K. Szalewicz, *Chem. Rev.* **1994**, *94*, 1887–1930; c) R. M. Parrish, L. A. Burns, D. G. A. Smith, A. C. Simmonett, A. E. DePrince, E. G. Hohenstein, U. Bozkaya, A. Y. Sokolov, R. Di Remigio, R. M. Richard, J. F. Gonthier, A. M. James, H. R. McAlexander, A. Kumar, M. Saitow, X. Wang, B. P. Pritchard, P. Verma, H. F. Schaefer, K. Patkowski, R. A. King, E. F. Valeev, F. A. Evangelista, J. M. Turney, T. D. Crawford, C. D. Sherrill, *J. Chem. Theory Comput.* **2017**, *13*, 3185–3197; d) R. M. Parrish, C. D. Sherrill, *J. Chem. Phys.* **2014**, *141*, 044115; e) R. M. Parrish, T. M. Parker, C. D. Sherrill, *J. Chem. Theory Comput.* **2014**, *10*, 4417; f) R. M. Parrish, C. D. Sherrill, *J. Am. Chem. Soc.* **2014**, *136*, 17386.
[39] K. Fujita, D. Muraoka, T. Ogawa, H. Kitamura, K. Suzuki, S. Saito, *Energy Procedia* **2014**, *63*, 863–870.

Manuscript received: December 15, 2022
Accepted manuscript online: January 31, 2023
Version of record online: February 24, 2023